BCSJ

Document type: Article

Selected Paper

Acceleration of Hydrolytic DNA Cleavage by Dicopper(II) Complexes with *p*-Cresol-Derived Dinucleating Ligands at Slightly Acidic pH and Mechanistic Insights

Masahito Kodera,* Yuki Kadoya, Kenta Aso, Katsuki Fukui, Akiko Nomura, Yutaka Hitomi, and Hiroaki Kitagishi

Department of Molecular Chemistry and Biochemistry, Doshisha University, Kyotanabe, Kyoto 610-0321, Japan

E-mail: mkodera@mail.doshisha.ac.jp

Received: November 17, 2018; Accepted: December 26, 2018; Web Released: January 22, 2019

Masahito Kodera

Masahito Kodera is a Professor at the Department of Molecular Chemistry and Biochemistry, Graduate School of Science and Engineering, Doshisha University. He received his Ph.D. at the Engineering Graduate School, Kyoto University in 1987. He started his career as an Assistant Professor at the Institute for Molecular Science in 1987, and moved to Kyushu University. He was an Assistant Professor at Kyushu University from 1988 to 1993, and moved to Doshisha University. He was Lecturer at Doshisha University from 1993 to 1994, Associate Professor from 1994 to 2001, and has been Professor from 2001 until now.

Abstract

Four dicopper(II) complexes, $[Cu_2(\mu\text{-}X)(bcmp)](ClO_4)_2$ [X = OH (**1a**) and X = Cl (**1b**)], $[Cu_2(\mu\text{-}OH)(Me_4bcmp)](ClO_4)_2$ (**2**), and $[Cu_2(bcc)](ClO_4)_3$ (**3**), were synthesized with three *p*-cresol-derived ligands, 2,6-bis(1,4,7-triazacyclononylmethyl)-4-meth-ylphenol (Hbcmp), 2,6-bis(1,4,7-triaza-4,7-dimethylcyclonon-ylmethyl)-4-methylphenol (HMe_4bcmp), and 2,6-bis(1,4,7,10-tetrazacyclododecylmethyl)-4-methylphenol (Hbcc) to study hydrolytic DNA cleavage. Crystal structures of **1a**, **1b**, **2**, and **3** were determined by X-ray analysis. The pH titrations and spectroscopic studies in the complexations of the ligands with copper(II) perchlorate revealed that the dicopper core structures of **1a**, **2**, and **3** in the solid state are kept at pH 5–9 in an aqueous solution. DNA binding abilities of **1a**, **2**, and **3** were examined by isothermal titration calorimetry (ITC). DNA cleavage studies were carried out by using supercoiled plasmid pUC19 DNA. **1a** largely accelerated hydrolytic DNA cleavage at pH 5–6 but not at pH 7–8. This is the first example of pH-dependent DNA cleavage by a dicopper complex. Inhibition studies with specific DNA binders, 4′,6-diamidino-2-phenylindole and methyl green, suggested that **1a** accelerates the DNA cleavage via GC-specific binding. The mechanistic insights into the pH-dependent DNA cleavage are proposed on the basis of the crystal structures, structures in aqueous solutions, DNA binding modes, and DNA cleavage activities of **1a**, **1b**, **2**, and **3**.

Keywords: Dicopper(II) complex | DNA cleavage | Mechanism

1. Introduction

Recently, there have been considerable interests in the development of metal complexes for medical purposes by blocking DNA replication through binding and/or cutting DNA.[1] Various platinum(II) complexes, cisplatin[2] and its derivatives, such as oxaliplatin,[3] lobaplatin,[4] and nedaplatin,[5] are used as anticancer drugs. Since these anticancer drugs are accompanied with heavy side-effects and resistance problems, metal complexes that bind and/or cut DNA of cancer cells selectively are required to solve these problems.

It is well known that the microenvironment in cancer cells is significantly different from that in normal cells.[6] As one of the key features of cancer cells, tumor extracellular pH is often acidic.[7] This is mainly caused by aerobic glycolysis. On the other hand, intracellular pH of tumors is neutral to alkaline.[7] Various dinuclear metal complexes capable of promoting hydrolytic DNA cleavage have been synthesized for the purpose of developing a new type of anticancer drugs.[1a–1c,8] Montagner reported that a dicopper(II) complex with Hbcmp $[Cu_2(\mu\text{-}OH)(bcmp)](NO_3)_2$ (**1c**) hydrolytically cleaved supercoiled plasmid pUC19 DNA (SC-DNA) at pH 8.2, and showed high cytotoxic activity to cancer cells, causing apoptosis.[9] The pH-dependent hydrolytic DNA cleavage by **1c**, however, has not been reported. The selective apoptosis of cancer cells by using pH-dependent DNA cleavage of metal complexes is desirable for the development of anticancer drugs that are less toxic, target specific, and with reduced side effects. Even if hydrolytic cleavage is reversible as repair enzymes repair DNA damage in cancer cells, pH-dependent hydrolytic DNA cleav-

age may provide a new concept for a DNA cleavage study as well as the development of anti-cancer drugs.

In this study, we synthesized four dicopper(II) complexes $[Cu_2(\mu\text{-OH})(bcmp)](ClO_4)_2$ (**1a**), $[Cu_2(\mu\text{-Cl})(bcmp)](ClO_4)_2$ (**1b**), $[Cu_2(\mu\text{-OH})(Me_4bcmp)](ClO_4)_2$ (**2**), and $[Cu_2(bcc)](ClO_4)_2$ (**3**) to study the pH-dependence of hydrolytic DNA cleavage by the dicopper complexes, and found that **1a** largely accelerated the hydrolytic cleavage of supercoiled plasmid pUC19 DNA at pH 5.0–6.0, but did not at pH 7.0–8.0. Since usually hydrolytic cleavage of DNA is accelerated under basic conditions, the large acceleration at pH 5–6 is quite an unusual example. For example, purple acid phosphatases specifically accelerate the hydrolysis of phosphate ester at acidic pH. Here, we propose mechanistic insights into the pH-dependent activity control in the hydrolytic DNA cleavage of **1a**.

2. Experimental

Materials. All ordinary reagents were purchased and used as received unless otherwise noted. A supercoiled plasmid pUC19 DNA was purchased from Nippon Gene CO., LTD. A 33 mer oligo DNA 5′-d(GAC TCC ACA GTG CAT ACG TGG GCT CCA ACA GGT)-3′ and the complementary strand were purchased from Thermo Fisher Scientific, from which a 33 mer double-strand DNA was prepared. Two *p*-cresol-derived ligands, 2,6-bis(1,4,7-triazacyclononylmethyl)-4-methylphenol (Hbcmp) and 2,6-bis(1,4,7,10-tetrazacyclododecylmethyl)-4-methylphenol (Hbcc) were prepared according to literature.[10]

Measurements. Elemental analyses (C, H, and N) were carried out on a Perkin-Elmer Elemental Analyzer 2400 II. UV-vis absorption spectra were recorded on an Agilent 8454 UV spectroscopy system. The pH measurement was carried out on a Horiba Laqua electrode. Electrospray ionization mass spectra (ESI MS) were recorded on a JEOL JMS-T100CS spectrometer. Infrared (IR) spectra were recorded on a Shimadzu Single Reflection HATR IR Affinity-1 MIRacle 10. ^{1}H NMR spectra were recorded on a JEOL ECA-500RX spectrometer using Me_4Si or TSP as an internal standard.

1-Tosyl-1,4,7-triazacyclononane. 1,4,7-Tritosyl-1,4,7-triazacyclononane (7.84 g, 13.2 mmol) and phenol (9.43 g, 100 mmol) were dissolved in 30% HBr solution in AcOH (110 mL). The solution was stirred for several hours at 30 °C until evolution of HBr ceased and then heated at 90 °C for 2 days. The HBr salt of the product generated was collected by filtration and washed with Et_2O. The solid was dissolved in 1.5 M aqueous NaOH (100 mL) and extracted with $CHCl_3$ (4 × 15 mL). The combined organic layer was dried over Na_2SO_4. After filtration and concentration, the product was obtained as white solid. Yield: 2.70 g (72%). ^{1}H NMR (500 MHz, $CDCl_3$); δ/ppm: 7.69 (d, $J = 8.0$ Hz, 2H, Ph), 7.31 (d, $J = 8.0$ Hz, 2H, Ph), 3.16–3.21 (m, 4H, CH_2), 3.05–3.11 (m, 4H, CH_2), 2.89 (s, 4H, CH_2), 2.43 (s, 3H, CH_3).

1,4-Dimethyl-7-tosyl-1,4,7-triazacyclononane. Formic acid (10 mL) and formaldehyde (10 mL) were added dropwise to a solution of 1-tosyl-1,4,7-triazacyclononane (2.62 g, 9.25 mmol) in H_2O (3 mL) at 0 °C. The mixture was stirred for 30 min, and refluxed at 110 °C for 15 h. To the resultant mixture was added 12 M HCl (6 mL), and concentrated to dryness. To the residue was added 1.5 M aqueous NaOH (20 mL) and extracted with $CHCl_3$ (4 × 20 mL). The extracts were combined and dried over Na_2SO_4. After filtration and concentration, the product was obtained as yellow solid. Yield: 2.83 g (98%). ^{1}H NMR (500 MHz, $CDCl_3$); δ/ppm: 7.67 (d, $J = 8.0$ Hz, 2H, Ph), 7.30 (d, $J = 8.0$ Hz, 2H, Ph), 3.21–3.29 (m, 4H, CH_2), 2.87–2.94 (m, 4H, CH_2), 2.69 (s, 4H, CH_2), 2.42 (s, 3H, CH_3), 2.40 (s, 6H, CH_3).

1,4-Dimethyl-1,4,7-triazacyclononane. 1,4-Dimethyl-7-tosyl-1,4,7-triazacyclononane (3.24 g, 10.4 mmol) was added to conc. H_2SO_4 (15 mL) and heated at 120 °C for 36 h under N_2. The mixture was cooled to room temperature, and 12 M aqueous NaOH was slowly added until pH became 10. Generated Na_2SO_4 was filtered off, and extracted with $CHCl_3$ (5 × 40 mL). The product was obtained from the extracts as yellow oil. Yield: 0.933 g (57%). ^{1}H NMR (500 MHz, $CDCl_3$); δ/ppm: 2.65–2.71 (m, 4H, CH_2), 2.50–2.57 (m, 8H, CH_2), 2.41 (s, 6H, CH_3).

2,6-Bis(*N*,*N*′-4,7-dimethyl-1,4,7-triazacyclonon-1-ylmethyl)-4-methylphenol Pentahydrochloride ($HMe_4bcmp\cdot5HCl$). 1,4-Dimethyl-1,4,7-triazacyclononane (0.365 g, 2.32 mmol) and 2,6-bis(chloromethyl)-4-methylphenol (0.215 g, 1.05 mmol) were dissolved in MeCN (40 mL) and Et_3N (0.34 mL, 2.44 mmol) was added. The solution was refluxed for 12 h under N_2. After concentration, the remainder was purified by column chromatography (alumina, $CHCl_3$/MeOH) to give 2,6-bis(*N*,*N*′-4,7-dimethyl-1,4,7-triazacyclonon-1-ylmethyl)-4-methylphenol as yellow oil. Yield: 0.330 g (70%). ^{1}H NMR (500 MHz, $CDCl_3$); δ/ppm: 6.87 (s, 2H, Ph), 3.72 (s, 4H, CH_2), 2.84–2.89 (m, 8H, CH_2), 2.63–2.69 (m, 16H, CH_2), 2.35 (s, 12H, CH_3), 2.23 (s, 3H, CH_3). The yellow oil product (1.19 g, 2.66 mmol) was dissolved in EtOH (27 mL) and 12 M HCl (9 mL) was added. The mixture was concentrated to dryness. After filtration and washing with EtOAc, the product was obtained as white solid. Yield: 1.41 g (2.24 mmol, 84%). Anal. calcd for $HMe_4bcmp\cdot5HCl\cdot5H_2O$: C, 41.76; H, 8.55; N, 11.69. Found: C, 41.69; H, 8.83; N, 12.22. ^{1}H NMR (500 MHz, D_2O); δ/ppm: 7.39 (s, 2H, Ph), 4.21 (s, 4H, CH_2), 3.10–3.79 (m, 24H, CH_2), 2.94 (s, 12H, CH_3), 2.34 (s, 3H, CH_3).

Dicopper Complexes 1a, 1b, 2, and 3. To a solution of Hbcmp (0.149 mmol) in H_2O (10 mL) was added a solution of $Cu(ClO_4)_2\cdot6H_2O$ (126.6 mg, 0.342 mmol) in H_2O (4 mL). The solution was neutralized with 1.0 M aqueous NaOH under N_2. After concentration, $[Cu_2(\mu\text{-OH})(bcmp)](ClO_4)_2$ (**1a**) was obtained as green solid and recrystallized from Et_2O/MeCN to give green crystals suitable for the X-ray analysis. Yield: 34.8 mg (44.5 µmol, 30%). Anal. calcd for $[Cu_2(\mu\text{-OH})bcmp](ClO_4)_2\cdot MeCN\cdot0.5H_2O$: C, 35.30; H, 5.41; N, 12.53. Found: C, 35.48; H, 5.50; N, 12.21. ESI MS (H_2O/MeCN m/z); $[\mathbf{1a} - ClO_4]^+$: 632.93. IR (KBr); $\tilde{\nu}$/cm^{-1}: 3586–2864, 1613, 1479, 1458, 1375, 1082. $[Cu_2(\mu\text{-Cl})(bcmp)](ClO_4)_2$ (**1b**) was obtained from Hbcmp·6HCl. Yield: 11.9 mg (31%). Anal. calcd for $[Cu_2(\mu\text{-Cl})bcmp](ClO_4)_2\cdot MeCN$: C, 34.88; H, 5.09; N, 12.38. Found: C, 35.00; H, 5.14; N, 12.20. ESI MS (H_2O/MeCN m/z); $[\mathbf{1b} - ClO_4]^+$: 650.89. $\tilde{\nu}$/cm^{-1}: 3620–2872, 1614, 1476, 1446, 1354, 1103. $[Cu_2(\mu\text{-OH})(Me_4bcmp)](ClO_4)_2$ (**2**) was obtained from HMe_4bcmp. Yield: 94.3 mg (52%). Anal. calcd for $[Cu_2(\mu\text{-OH})Me_4bcmp](ClO_4)_2\cdot MeCN\cdot2H_2O$: C, 37.46; H, 6.17; N, 11.33. Found: C, 37.72; H, 6.26; N, 11.08. ESI-MS (H_2O/MeCN m/z); $[\mathbf{2} - ClO_4]^+$: 689.04. $\tilde{\nu}$/cm^{-1}: 3613–2868, 1614, 1481, 1472, 1431, 1366, 1082. $[Cu_2(bcc)](ClO_4)_3$ (**3**) was obtained from Hbcc and recrystal-

lized from Et_2O/MeCN/MeOH. Yield: 0.119 g (50%). Anal. calcd for $[Cu_2bcc](ClO_4)_3 \cdot MeOH \cdot 1.5H_2O$: C, 32.52; H, 5.67; N, 11.67. Found: C, 32.46; H, 5.41, N; 11.81. ESI MS (H_2O/MeCN m/z); $[\mathbf{3} - ClO_4]^+$: 801.12, $[\mathbf{3} - 2ClO_4]^{2+}$: 351.08. $\tilde{\nu}/cm^{-1}$: 3620–293, 1616, 1470, 1441, 1381–1306, 1099.

Structure Determination of Single Crystals. The crystal structures of **1a**, **1b**, **2** and **3** were determined on a Rigaku R-AXIS RAPID diffractometer using multi-layer mirror monochromated Cu-Kα radiation. The data were collected at a temperature of -160 ± 1 °C or -180 ± 1 °C to a maximum 2θ value of 136.5°. The linear absorption coefficient, μ, for Cu-Kα radiation is 31.825, 38.394, 39.633, or 44.927 cm^{-1}. An empirical absorption correction was applied. The data were corrected for Lorentz and polarization effects. Crystallographic data of the complexes are shown in Table S1. Crystallographic data reported in this manuscript have been deposited with Cambridge Crystallographic Data Centre as supplementary publication no. CCDC-000000. Copies of the data can be obtained free of charge via CCDC Website.

pH Change and Spectral Studies in Complexation of Hbcmp, HMe_4bcmp, and Hbcc. A solution of each ligand (0.5 mM) and $Cu(ClO_4)_2 \cdot 6H_2O$ (1.0 mM) in H_2O (2.0 mL) was placed in a cuvette, and titrated with an aqueous NaOH (0.05 M) at 25 °C. The pH change was monitored on a pH meter. The electronic absorption and ESI MS spectra were measured using the same solution after measuring pH.

Isothermal Titration Calorimetry (ITC). ITC measurements were performed at 37 °C on a Malvern MacroCal VP-ITC. The solution of the 33 mer oligo ds-DNA (25 μM) in a buffered aqueous solution ((MES, 10 mM) containing NaCl (10 mM)) was prepared in the cell. The solution of **1a**, **2**, or **3** (1.0 mM) in a buffered aqueous solution (MES, 10 mM) containing NaCl (10 mM) was prepared in the syringe. The 25 aliquots (10 μL each) of the solution of **1a**, **2**, or **3** were added into the DNA solution to measure the heat of complexation. The raw data was corrected by subtracting the heat of dilution, and the titration curve thus obtained was analyzed using ORIGIN software. Each ITC data was collected by two independent measurers and the reproducible data was employed.

DNA Cleavage Study. DNA cleavage activity of **1a**, **1b**, **2**, and **3** were evaluated by using pUC19 DNA and followed by agarose gel electrophoresis. pUC19 DNA (0.50 μg/μL) was incubated with the dicopper complex (10 μM) in an aqueous buffer solution (10 mM, pH 5.0, 5.5, 5.9, 6.0 (MES), 7.4 (Tris-HCl), and 8.2 (TAPS)) containing NaCl (10 mM) at 37 °C in the dark. An aliquot was taken from the solution at 0, 1, 2, 5, and 10 h, and the reaction was quenched upon addition of loading buffer (0.025% bromophenol blue, 0.025% xylene cyanol FF, 1.0 mM EDTA and 30% glycerol). Each sample was loaded onto a 1% agarose gel in TAE (Tris/acetate/EDTA) buffer. The gels were subjected to electrophoresis for 1 h at 100 V, followed by staining with ethidium bromide (0.5 μg/mL) for 1 h. Gel bands were visualized using UV transilluminator and photographed using a Vilber Lourmat ECX-20-M, and were quantified using a correction factor of 1.06 for the reduced stain uptake of Form I. All data for the conversion of Form I to Form II are shown in Figure S5–S13 and Table S4–S12.

Inhibition of the DNA Cleavage of 1a. pUC19 DNA (0.50 μg/μL) was dissolved in an aqueous buffer solution (10 mM, pH 5.0 and 5.5 (MES)) containing NaCl (10 mM) in the presence of DAPI or methyl green (5, 10, 50 μM), and **1a** (10 μM) was added and incubated at 37 °C for 1 h in the dark. Progress of the reaction was evaluated as shown in the DNA cleavage study.

3. Results and Discussion

Syntheses and Structures of Dicopper Complexes. The chemical structures of 2,6-bis(1,4,7-triazacyclononylmethyl)-4-methylphenol (Hbcmp), 2,6-bis(1,4,7-triaza-4,7-dimethylcyclononylmethyl)-4-methylphenol (HMe_4bcmp), and 2,6-bis-(1,4,7,10-tetrazacyclododecylmethyl)-4-methylphenol (Hbcc) are shown in Scheme 1. Hbcmp and Hbcc have triazacyclononane (tacn) and tetraazacyclododecane (cyclen) as pendant groups at 2,6-positions of the *p*-cresol moiety, respectively, and prepared according to the literature.[10] HMe_4bcmp is a new ligand where four macrocyclic NH groups of Hbcmp are fully methylated. The synthetic route of HMe_4bcmp is shown in Scheme 2. These ligands form dicopper(II) complexes $[Cu_2(\mu\text{-}X)(bcmp)](ClO_4)_2$ [X = OH (**1a**) and X = Cl (**1b**)], $[Cu_2(\mu\text{-}OH)(Me_4bcmp)](ClO_4)_2$ (**2**), and $[Cu_2(bcc)](ClO_4)_3$ (**3**). The complexes were structurally characterized by X-ray analysis, and characterized by elemental analysis and various spectroscopic measurements. As described below, the ligands stabilize the dinuclear structures at pH 5–9 in an aqueous solution.

ORTEP views of **1a**, **1b**, **2**, and **3** are shown in Figure 1. The crystallographic data are shown in Table S1, and the selected bond distances and angles are shown in Table S2. In **1a**, two Cu(II) ions are incorporated into a bcmp ligand with the μ-OPh-μ-OH double bridge, where each Cu ion takes distorted square pyramidal geometry with three *N*-atoms of a pendant tacn and two *O*-atoms of the μ-OPh-μ-OH bridge. **1b** is structurally almost the same as **1a** but μ-OH of **1a** is replaced by μ-Cl. In **2**, two Cu(II) ions are incorporated into a Me_4bcmp ligand with the μ-PhO-μ-OH double bridge. The overall structures of **1a** and **2** are almost the same except for NCH_3

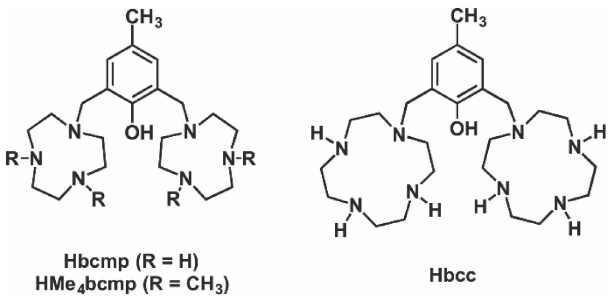

Scheme 1. Chemical structures of supporting ligands.

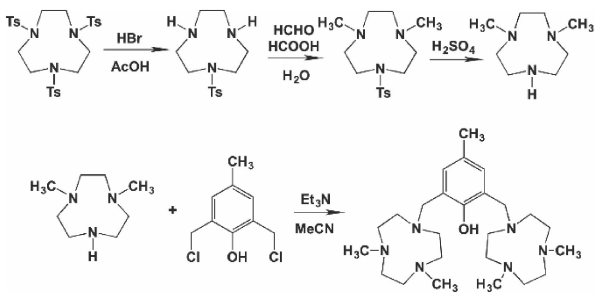

Scheme 2. Synthetic scheme of H_2Mebcmp.

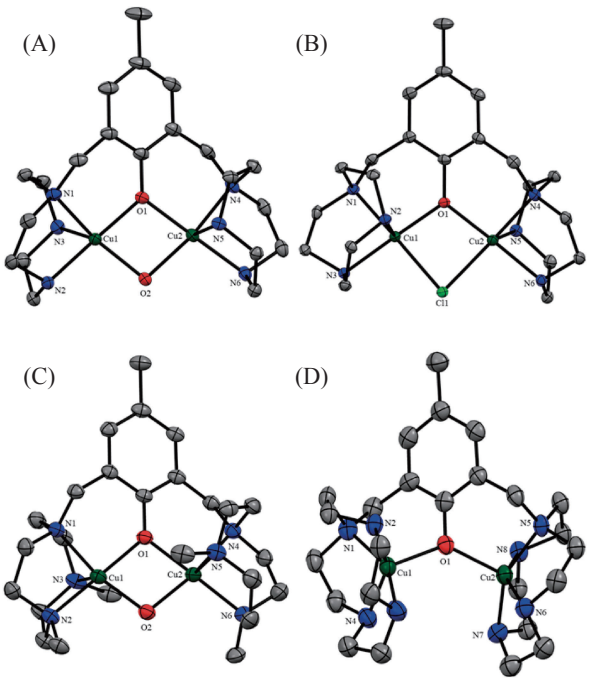

Figure 1. ORTEP diagrams of the cationic parts of (A) **1a**, (B) **1b**, (C) **2**, and (D) **3** (ORTEP plot; unlabeled open ellipsoids represent carbon atoms).

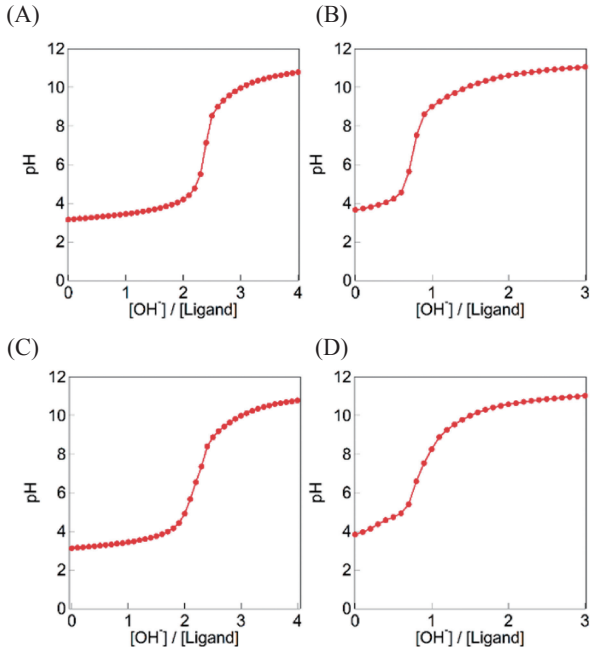

Figure 2. pH change of an aqueous solution containing each ligand (0.5 mM), (A) **Hbcmp**, (C) **HMe$_4$bcmp**, or (D) **Hbcc**, and $Cu(ClO_4)_2 \cdot 6H_2O$ (1.0 mM) upon titration with an aqueous NaOH solution (0.05 M) at 25 °C. In the case of (B), **1b** was used instead of the ligand, and the pH change was monitored in the same way.

groups in **2**. In **3**, two Cu(II) ions are incorporated into a bcc ligand with the μ-PhO bridge, and each Cu takes square pyramidal geometry with four *N*-atoms of a pendant cyclen and a *O*-atom of the μ-OPh bridge. The Cu···Cu distances of **1a** and **2** are 2.9985(7) and 3.033(1) Å, close to each other, but shorter than 3.878(1) Å of **3**. This may reflect differences of the bridging structures where the μ-PhO-μ-OH doubly bridged structures of **1a** and **2** shorten the Cu···Cu distances as compared with the μ-PhO singly bridged one of **3**. The coordination geometry is examined by the τ-values that vary from 0, for an idealized square pyramidal, to 1, for an idealized trigonal bipyramidal.[11] The τ-values, $\tau_{Cu(1)} = 0.243$ and $\tau_{Cu(2)} = 0.228$ for **1a**, $\tau_{Cu(1)} = 0.217$ and $\tau_{Cu(2)} = 0.206$ for **2**, and $\tau_{Cu(1)} = 0.038$ and $\tau_{Cu(2)} = 0.066$ for **3**, show that **1a** and **2** are distorted square pyramidal similar to each other and **3** is regular square pyramidal.

In spite of the similar bridging structures of **1a** and **2**, the accessibility to the μ-OH group is significantly different. The *O*-atom of μ-OH in **1a** protrudes by 0.842 Å from the mean plane defined by four *N*-atoms of macrocyclic NH groups (Figure S1), clearly showing that the μ-OH group is easy to access from outside. On the other hand, the *O*-atom of μ-OH in **2** is surrounded by the NCH_3 groups that sterically hinder the access to the μ-OH group, where the deviation of the *O*-atom of μ-OH from the mean plane defined by four *C*-atoms of NCH_3 groups is 0.001 Å (Figure S1). Moreover, the Cu-$O_{\mu\text{-OH}}$ bond distances 1.971(2) and 1.980(3) Å of **1a** are significantly longer than 1.930(3) and 1.925(4) Å of **2**. These data indicate that the μ-OH bridge of **1a** weakly bonds to two Cu(II) ions. These structural features suggest that the μ-OH bridge of **1a** is more reactive in the nucleophilic attack to an external substrate such as a phosphate moiety of DNA than that of **2**.

Dicopper Core Structures at pH 5–9 in an Aqueous Solution. To examine dicopper core structures at pH 5–9 in an aqueous solution, complexations of the ligands were monitored by pH and spectroscopic measurements. To an aqueous solution of a 1:2 mixture of each ligand and $Cu(ClO_4)_2 \cdot 6H_2O$ was added standardized aqueous NaOH, and the pH change was monitored on a pH meter and the electronic absorption and electrospray ionization mass (ESI MS) spectra were measured. The plots of the pH change vs molar equivalent of NaOH added are shown in Figure 2. The electronic absorption and ESI MS spectra at various pH are shown in Figures S2 and S3, respectively.

In the complexations of Hbcmp and HMe$_4$bcmp, 2 eq of OH^- was consumed by pH 5.0 as shown in Figure 2(A) and (C). This can be assigned to the release of two protons belonging to the phenol of each ligand and to a H_2O bonded to dicopper(II) core to form μ-OPh-μ-OH bridge. This is consistent with p*K*a value of the H_2O bonded to the dicopper(II) core, 4.69, reported for **1c**.[9] The electronic absorption spectra in complexation of Hbcmp and HMe$_4$bcmp at pH 5–9 are almost the same as those of **1a** and **2** in an aqueous solution, respectively (Figure S2). The spectra of **1a** and **2** exhibit two bands at around 340–380 nm assignable to phenoxo-Cu(II) and hydroxo-Cu(II) LMCT (ligand-to-metal charge transfer) bands, taking account of the reported data that the LMCT bands appear at 350–400 nm in related dicopper(II) complexes.[12] Moreover, the bridging structures of **1a** and **2** are confirmed by the ESI MS spectra shown in Figure S3. The ESI MS spectra of **1a** and **2** at pH 5–9 in aqueous solutions show the major peaks at m/z 632 and 689 corresponding to $[bcmp + 2Cu(II) + OH + ClO_4]^+$

and $[Me_4bcmp + 2Cu(II) + OH + ClO_4]^+$, respectively. These results show that the μ-OPh-μ-OH bridges of **1a** and **2** are kept at pH 5–9. Upon addition of aqueous NaOH to **1b** in an aqueous solution, 1 eq of OH^- was consumed by pH 5.0, (Figure 2(B)), showing that μ-Cl of **1b** was replaced by μ-OH, and thus, **1b** is converted to **1a** in an aqueous solution.

In the complexation of Hbcc, 1 eq of OH^- was consumed by pH 5.0 (Figure 2(D)). The electronic absorption spectra in the complexation of Hbcc at pH 5–9 are the same as that of **3** in an aqueous solution (Figure S2), which exhibits a weak band at 410 nm assignable to the phenoxo-Cu(II) LMCT.[13] The ESI MS spectra of **3** at pH 5–9 in an aqueous solution show the major peak at m/z 801 corresponding to $[bcc + 2Cu(II) + 2ClO_4]^+$ (Figure S3). These results show that the μ-OPh bridged structure of **3** is kept at pH 5–9 in an aqueous solution.

Thus, the μ-OPh-μ-OH bridges of **1a** and **2** and the μ-OPh bridge of **3** are kept intact at pH 5–9 in H_2O. It was reported that the μ-OPh-μ-OH bridge is kept intact at pH 5–12 in dicopper(II) complex with 2,6-bis(dipyridylmethylaminomethyl)-4-methyl-phenol, a *p*-cresol-derived heptadentate dinucleating ligand.[14a] Thus, the μ-OPh-μ-OH bridging structures are common in the dicopper(II) complexes with the *p*-cresol-derived heptadentate ligands in the wide range of pH. On the other hand, the μ-OPh singly bridged structure of **3** is kept with the bcc ligand under the same conditions.

DNA Binding of Dicopper(II) Complexes. The pH and structural effect on the DNA binding ability of **1a**, **2**, and **3** were explored by isothermal titration calorimetry (ITC). By the ITC measurement, the binding enthalpy ($\Delta H°$) is directly obtained, and the entropy ($\Delta S°$) and the binding constant (K) are derived from curve fitting and free energy relationship. A linear 33 mer oligo double-stranded DNA was used for the measurement of the DNA binding constant where the hydrolytic DNA cleavage by the dicopper complexes can be eliminated because of the low reactivity of linear DNA. The isothermal calorimetric titration curves were recorded for the titration of **1a** into the 33 mer oligo double-stranded DNA solution in 10 mM of MES buffer at pH 5.0, 5.5, and 6.0 in the presence of NaCl (10 mM) to keep a constant ionic strength. Moreover, the titration curves for DNA binding of **2** and **3** were obtained at pH 6.0 under the same conditions. The thermodynamic parameters, $\Delta H°$, $\Delta S°$, and K, are shown in Table S3. Negative $\Delta H°$ and positive $\Delta S°$ were obtained in all measurements, showing that DNA binding of **1a**, **2**, and **3** are enthalpically and entropically favorable. The ITC profiles and the corresponding molar ratio plots are shown in Figure 3.

The DNA binding constants of **1a** determined at pH 5.0, 5.5, and 6.0 are $1.81 \pm 0.84 \times 10^5$, $1.23 \pm 0.43 \times 10^5$, and $1.05 \pm 0.20 \times 10^5\,M^{-1}$, respectively (Table S3), and slightly increasing with lowering pH, indicating that a binding complex of **1a** with DNA is stabilized by the protonation. Since the structure of **1a** is kept intact at pH 5.0–9.0 in an aqueous solution, **1a** is not protonated in the pH domain. Thus, the protonation occurs in the binding complex of **1a** with DNA. The $\Delta H°$ and $\Delta S°$ values obtained at pH 5.0, 5.5, and 6.0 are -0.57 ± 0.08, -1.08 ± 0.24, and -1.39 ± 0.19 (kcal·mol^{-1}) and 22.2, 19.8, and 18.5 (cal·mol^{-1}·K^{-1}), respectively (Table S3). Both $\Delta H°$ and $\Delta S°$ values increased with lowering pH, suggesting that the protonation may occur at the phosphate moiety of the DNA

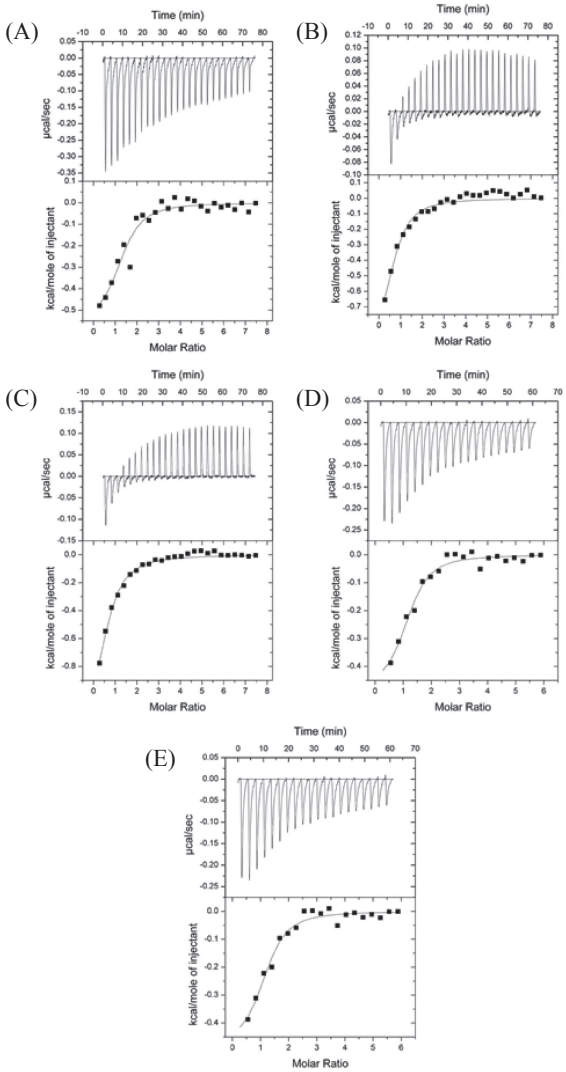

Figure 3. Isothermal calorimetric titration curves: **1a** at pH 5.0 (A), 5.5 (B), 6.0 (C), **2** at pH 6.0 (D), and **3** at pH 6.0 (E). Experimental conditions: A solution of **1a** (1 μM) in a syringe was added, in an equal interval 25 times, to a solution of the linear 33 mer ds-DNA (25 μM) in the cell in the presence of NaCl (10 mM) in an aqueous buffer solution at pH 5.0, 5.5, and 6.0 (MES, 10 mM) at 37 °C. In the case of **2** and **3**, titrations were conducted in the same manner at pH 6.0 (MES, 10 mM).

main chain in the binding complex to induce dehydration. Thus, the increase in the binding constant of **1a** with DNA at low pH is entropy-driven.

Moreover, the DNA binding abilities of **2** and **3** may be explained from both hydrophobic and electrostatic interactions with DNA. The DNA binding constants of **2** and **3** determined at pH 6.0 are $2.64 \pm 0.97 \times 10^5$, and $2.63 \pm 0.53 \times 10^5\,M^{-1}$, respectively (Table S3). These values are almost the same. Interestingly, however, the $\Delta H°$ and $\Delta S°$ values, -0.48 ± 0.06 (kcal·mol^{-1}) and 23.2 (cal·mol^{-1}·K^{-1}) for **2**, and -2.26 ± 0.11 (kcal·mol^{-1}) and 17.5 (cal·mol^{-1}·K^{-1}) for **3**, are largely different between **2** and **3**. The increase of entropy shows the increase of degree of freedom in the system. Therefore, the largest $\Delta S°$ value 23.2 indicates that hydrophobic interaction of

2 with DNA plays a key contribution in the complexation where dehydration from **2** and DNA causes the $\Delta S°$ value. The hydrophobic interaction is important because **2** is the most hydrophobic in **1a**, **1b**, **2**, and **3**. The negative enthalpy shows the formation of some new bonds including H-bond and electrostatic interaction. In this case, the least exothermic $\Delta H°$ value −0.48 in the complexation of **2** with DNA indicates that the bonding interactions are not so important. This is reasonable because **2** does not have NH groups capable of forming H-bonds. On the basis of the same consideration, $\Delta H°$ and $\Delta S°$ values −2.26 and 17.5 in complexation of **3** with DNA clearly show that H-bond and electrostatic interaction largely contribute, and the hydrophobic interaction is not so important. This is reasonable because **3** has six NH groups with net charge 3+, and thus, the most hydrophilic. The $\Delta H°$ values of **1a**, **2**, and **3** at pH 6 are −1.39, −0.48, and −2.26, respectively. **1a** and **3** are more exothermic than **2**. This shows that the H-bonding interactions of the NH groups play a key role in the DNA binding. Thus, the chemical understandings of the DNA binding abilities are deduced from thermodynamic parameters $\Delta H°$ and $\Delta S°$. Moreover, these results show that the interaction of **1a**, **2**, and **3** with DNA is controlled with chemical modifications of the pendant macrocyclic groups.

Acceleration of Hydrolytic Cleavage of Supercoiled Plasmid pUC19 DNA with Dicopper(II) Complexes in Slightly Acidic pH. Montagner et al. reported that **1c** promoted hydrolytic cleavage of supercoiled plasmid pUC19 DNA (SC-DNA, Form I) in an aqueous buffer solution at pH 8.2 at 37 °C,[9] and that the reaction was dependent on concentration of **1c** where at 50 μM of **1c**, almost complete nicking of Form I to Form II was observed in 3 h, but at 5 μM of **1c**, Form II was not observed. In our study, the reaction of SC-DNA with **1a** (10 μM) was examined at 37 °C in aqueous solutions at pH 5.0, 5.5, 5.9, 6.0, 7.4, and 8.2. In the absence of the dicopper(II) complex, the DNA cleavage was not observed at all as shown in Figure 4(A) of the blank experiment. Time courses of the decrease of Form I in the reaction of **1a** at pH 5.0–8.2 are shown in Figure 4(B). The DNA cleavage was largely accelerated at pH 5.0–6.0. By using such a small amount, 10 μM, of **1a**, 80% conversion of Form I to Form II was attained at pH 5.0 for 5 h. Interestingly, however, no DNA cleavage activity was observed at pH 7.4 and 8.2. Tris buffer used at pH 7.4 is known to coordinate Cu(II) ion,[14b] but in our case, gave no influence because the electronic spectra of **1a** in aqueous solutions using MES, Tris-HCl, and TAPS as buffer were completely the same each other. As shown in Figure 4(C), **1b** shows exactly the same activity as **1a**. This is because **1b** is rapidly converted to **1a** at pH 5–9 in an aqueous solution.

To examine the possibility of oxidative DNA cleavage by **1a**, the reaction was carried out in the presence of H_2O_2 (100–500 μM), but no acceleration occurred (Figure S4). Moreover, it was examined in the presence of NaN_3 and dimethyl sulfoxide that are known to inhibit oxidative DNA cleavage by singlet oxygen and hydroxyl radical, respectively, but the DNA cleavage of **1a** was not inhibited (Figure S4). Thus, it is demonstrated that the reaction of **1a** is not the oxidative DNA cleavage.

This is the first example of pH-dependent acceleration of hydrolytic DNA cleavage by synthetic metal complex. As

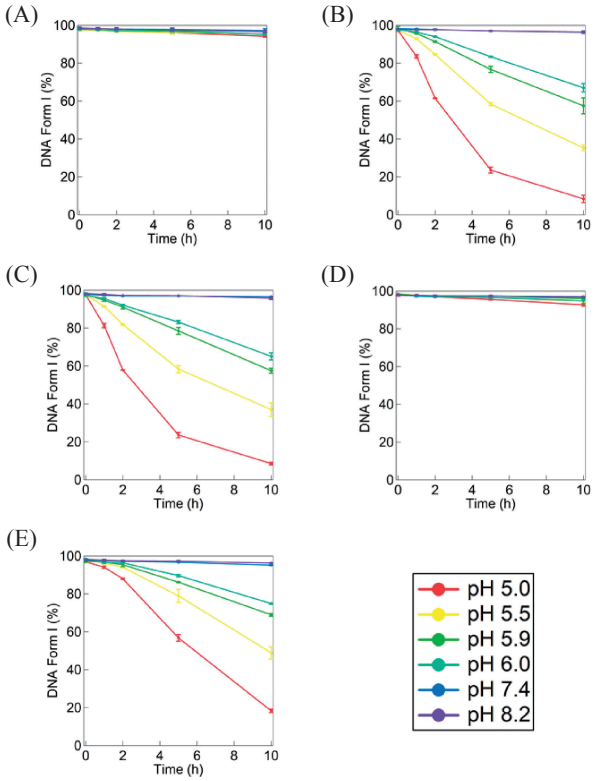

Figure 4. pH-dependent profile for DNA cleavage promoted by (A) Blank, (B) **1a**, (C) **1b**, (D) **2**, and (E) **3**, respectively. Experimental conditions: [NaCl] = 10 mM, [buffer] = 10 mM (pH 5.0, 5.5, 5.9, 6.0 (MES), 7.4 (Tris-HCl), and 8.2 (TAPS)), [pUC19 DNA] = 50 μMbp, [complex] = 10 μM at 37 °C for 0, 1, 2, 5, and 10 h. Experiments were carried out at least three times.

one of the distinctive natures of cancer cells, it is known that pH[7a–7c] and concentrations of reactive oxygen species (ROS)[15] in cancer cells are significantly different from those in normal cells. If we could control DNA cleavage activity of metal complexes depending on pH and ROS concentrations, it may serve to develop new types of anti-cancer drugs that selectively kill cancer cells but not normal cells. Therefore, pH-dependent acceleration of the hydrolytic DNA cleavage by **1a** may provide some insight into the development of a new type of anti-cancer drugs to reduce side-effects. It is necessary to investigate the cytotoxicity of **1a** to cancer cells in our future study.

Inhibition of DNA Cleavage with Specific DNA Binders. As estimated from the DNA binding constant of **1a**, ca 80–90% of the total amount of **1a** used bonds to DNA under the reaction conditions. Thus, it may be reasonable that the large acceleration of the hydrolytic DNA cleavage by **1a** is attained via the specific binding to DNA.

There are mainly four modes in non-covalent binding of metal complexes to ds-DNA, an intercalation, an electrostatic interaction with the DNA main chain, and a minor or a major groove binding. It is known that metal complexes having about a thousand molecular weight are suitable for the minor groove binding because of groove size.[16] Generally, the minor groove binders have crescent-shape structures with cationic centers at

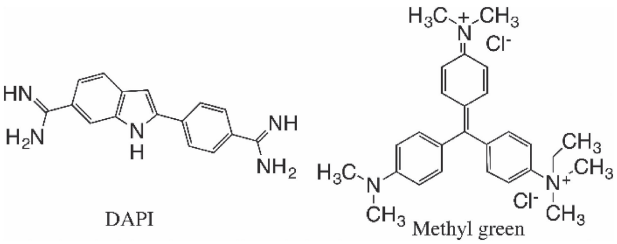

Figure 5. Chemical structures of 4′,6-diamidino-2-phenylindole (DAPI) and methyl green.

the both ends of compounds. These structural features match the overall structure of **1a**. The major groove binding may be possible but not so important because the molecular size of **1a** is much smaller than the space of the major groove. To clarify a DNA binding mode of **1a**, we carried out inhibition experiments using 4′,6-diamidino-2-phenylindole (DAPI),[17] a minor groove binder, and methyl green,[18] a major groove binder. The chemical structures of DAPI and methyl green are shown in Figure 5.

Time courses in the DNA cleavage of **1a** (10 μM) in the presence of DAPI (5.0–50 μM) at pH 5.0 are shown in Figure 6(A). The inhibition rates at 10 h are estimated from these data as 19, 50, and 87% in the presence of 10, 20, and 50 μM of DAPI, respectively, and increases with increase of the concentration of DAPI. Thus, the DNA cleavage of **1a** is inhibited by DAPI. The inhibition rates, however, are too small, considering from DNA binding constants, $4.7 \pm 0.3 \times 10^6\,M^{-1}$ reported for DAPI with ct-DNA in pH 5.0 acetate buffer at 25 °C[19] and $1.81 \pm 0.84 \times 10^5\,M^{-1}$ determined in this study for **1a** with a linear 33 mer oligo ds-DNA in pH 5.0 MES buffer at 37 °C. The binding constant of DAPI is nearly 25-fold larger than that of **1a**. This means that the DNA cleavage of **1a** may be almost completely inhibited in the presence of the same concentration of DAPI. The inhibition rate, however, was only 19% at the same concentration of DAPI. It is known that DAPI strongly bonds to DNA at the AT-rich site as a minor groove binder but weakly at the GC-rich site as an intercalator.[20] The binding constant of DAPI with GC-DNA was reported to be $1.2 \times 10^5\,M^{-1}$,[20] slightly smaller than $1.81 \times 10^5\,M^{-1}$ of **1a**. The low inhibition rate of DAPI can be explained from these binding constants, and thus, DAPI blocks the DNA binding of **1a** at GC-site. Therefore, acceleration of the DNA cleavage by **1a** may be attained through intercalation to the GC-site.

The results of inhibition experiments using a major groove binder, methyl green, are shown in Figure 6(B). The inhibition rates at 10 h are 12, 26, and 64% in the presence of 10, 20, and 50 μM of methyl green, and slightly lower than 19, 50, and 87% by DAPI. Thus, DAPI is a stronger inhibitor than methyl green. Methyl green is a major groove binder,[17b] and reported to retard DNA cleavage of deoxyribonuclease I, a minor groove binder.[17b] Thus, methyl green inhibits DNA binding of **1a** at the major groove, and also retards DNA cleavage of **1a** at the minor groove. This may be the reason for the relatively weak inhibition of methyl green compared with DAPI.

It may be reasonable that a cresol moiety of **1a** acts as an intercalator. The cresol ring of **1a**, however, is smaller than the aromatic ring of DAPI. From the DNA binding studies, it was

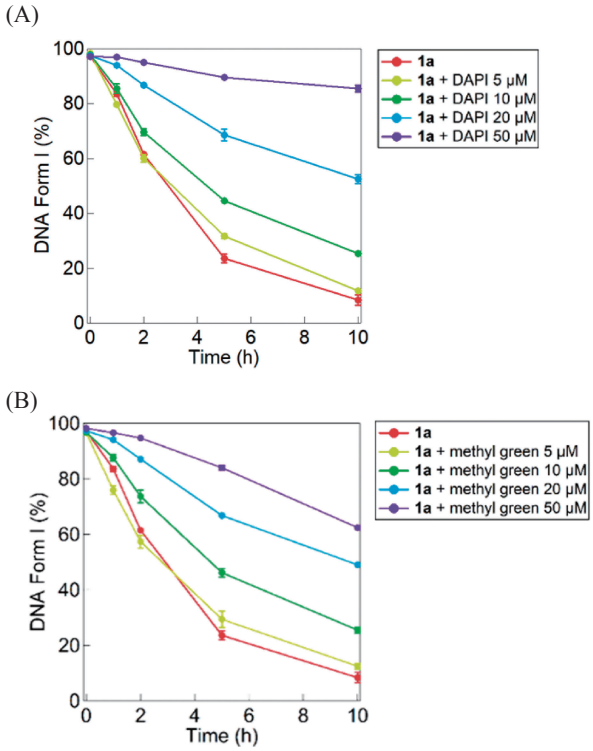

Figure 6. DNA cleavage by **1a** in the presence of (A) DAPI and (B) methyl green at pH 5.0. Experimental conditions: [NaCl] = 10 mM, [buffer] = 10 mM (MES), [pUC19 DNA] = 50 μM bp, [**1a**] = 10 μM, and [DAPI] = [methyl green] = 5, 10, 20, and 50 μM at 37 °C for 0, 1, 2, 5, and 10 h. Experiments were carried out at least three times.

shown that the NH groups of **1a** form H-bonds with a phosphate moiety of the DNA main chain. Thus, the DNA binding ability of **1a** is enhanced by not only the intercalation of a cresol moiety but also the H-bonds of the NH groups.

Mechanistic Insights into the pH-Dependent Activity Control in Hydrolytic DNA Cleavage of 1a. Purple acid phosphatases are widely distributed enzymes in biological systems, and catalyze hydrolytic cleavage of phosphate ester at slightly acidic pH.[21] This has a μ-OH bridged dimetal active center where the μ-OH bridge directly attacks phosphate ester as a nucleophile to accelerate hydrolysis.[22] Thus, it is likely that the μ-OH bridge is a key structure responsible for the large acceleration of hydrolytic DNA cleavage of **1a**. So, we examined the DNA cleavage of **2**, having a μ-OH bridge similar to **1a**, under the same reaction conditions to gain some insight into the mechanism of the acceleration in the hydrolytic DNA cleavage. As shown by time courses of decrease of Form I (Figure 4(D)), however, **2** showed no activity in the DNA cleavage at pH 5–8. The hydrolytic DNA cleavage activities of **1a** and **2** are totally different from each other in spite of similar bridging structures. This drastic difference may be explained by nucleophilicity of the μ-OH bridge and neighboring-group participation of the NH groups in **1a**. As shown by the crystal structures of **1a** and **2**, the μ-OH bridge of **1a** protrudes from the mean plane defined by four *N*-atoms of the NH groups by 0.842 Å, and thus, can easily access the phosphate ester in DNA. On the other hand, the μ-OH bridge of **2** is difficult to

access due to the steric hinderance of the NCH_3 groups. The nucleophilicity of the μ-OH bridge may be responsible for the difference of the DNA cleavage activity between **1a** and **2**. Thus, it is proposed that the DNA cleavage of **1a** proceeds through the nucleophilic attack of the μ-OH bridge.

Neighboring-group participation by the macrocyclic NH groups of **1a** may play a key role in the DNA cleavage. This is reasonable because they enforce the DNA binding of **1a** through the H-bonds as described in the DNA biding studies. Moreover, it is well-known that NH groups located near the metal center can accelerate the metal complex-based hydrolytic cleavage of phosphate esters.[23] In this situation, in order to clarify the role of the macrocyclic NH groups, **3** that has six NH groups was used for the DNA cleavage. Time courses in the reactions of **3** at pH 5.0–8.2 are shown in Figure 4(E). In the comparison of the time courses shown in Figure 4(B) and (E), **1a** is more reactive than **3**. The relatively low reactivity of **3** may be due to the absence of the μ-OH bridge. This further supports that the μ-OH bridge is responsible for the DNA cleavage. Interestingly, however, **3** accelerated the DNA cleavage without a μ-OH bridge, where the NH groups can activate a phosphate ester of the DNA main chain by the H-bonds and hydrolytic DNA cleavage may be attained by nucleophilic attack of H_2O molecule. On the other hand, in **2**, the NCH_3 groups do not form the H-bond to the phosphate ester, resulting in almost no activity of **2** in the DNA cleavage. In the comparison of DNA cleavage activity among **1a**, **2**, and **3**, it is proposed that both the μ-OH bridge and the NH groups are the key structures for the hydrolytic DNA cleavage.

One of the mechanistic insights deduced from the DNA binding studies is that the dehydration occurs by the protonation to the phosphate moiety in the DNA binding complex of **1a**. Another mechanistic insight is the H-bonding interaction of the NH groups in **1a** to the phosphate diester in the DNA main chain to potentially activate it for the DNA cleavage. The mechanism proposed on the basis of these features is shown in Figure 7. In the first step of the hydrolytic DNA cleavage, **1a** binds to the GC-site as an intercalator to form the DNA binding complex. The DNA binding complex is stabilized by H-bonds of the NH groups with a phosphate moiety in the DNA main chain. In this stage, the binding complex is weakly protonated and entropically stabilized by dehydration, and the phosphate diester is activated by the protonation for hydrolytic cleavage. The protonation may decrease the transition energy in the nucleophilic attack of the μ-OH bridge to the phosphate ester. Here, the large acceleration of the hydrolytic DNA cleavage of **1a** at pH 5–6 is also explained from the p*K*a values of phosphate monoester. The pKa_1 and pKa_2 values of deoxyribose-phosphate monoester are reported to be 1–2 and 5–6, respectively.[24] The pKa_2 value, 5–6, is exactly the same as the pH value at which the hydrolytic DNA cleavage of **1a** is accelerated. Thus, stabilization of the product monoester is the driving force of the large acceleration of the DNA cleavage by **1a** at pH 5–6. Finally, the dicopper complex is released from the product monoester. Thus, it is proposed that hydrolytic DNA cleavage of **1a** proceeds through the three steps as follows, (1) the DNA binding, (2) the stabilization of the transition state by protonation to give the phosphate monoester, and (3) the release of **1a**.

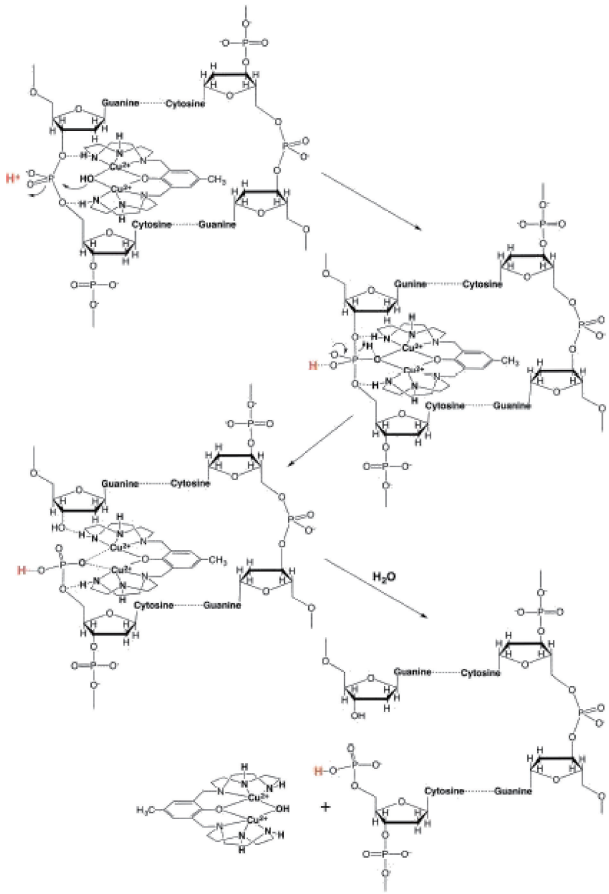

Figure 7. Proposed mechanism of the hydrolytic DNA cleavage by **1a**.

4. Conclusion

In this study, we synthesized dicopper complexes, **1a**, **1b**, **2**, and **3** with three *p*-cresol-derived ligands. The crystal structures revealed that overall structures of **1a** and **2** are similar but the accessibility to the μ-OH bridge is different. The dicopper core structures in the crystals are kept at pH 5–9 in an aqueous solution as shown by pH titrations and spectroscopic measurements in the complexations of the ligands with Cu(II) ions upon addition of a standardized aqueous NaOH. DNA binding mode of **1a** was examined by ITC measurements and inhibition experiments with specific DNA binders DAPI and methyl green, showing that **1a** bonds to DNA at the GC-site as an intercalator with assistance of the H-bond of the NH groups to a phosphate moiety in the DNA main chain. Moreover, the thermodynamic parameters, $\Delta H°$, $\Delta S°$, and K, indicated that the DNA binding is entropically and enthalpically favorable and the binding ability of **1a** is slightly enhanced by the protonation at pH 5–6. **1a** accelerated cleavage of supercoiled plasmid pUC19 DNA from Form I to Form II at pH 5–6. This is the first example of large acceleration of hydrolytic DNA cleavage by synthetic metal complexes at pH 5–6, though purple acid phosphatases accelerate hydrolysis of phosphate ester at acidic conditions. The comparison of the DNA cleavage activity among **1a**, **2**, and **3** revealed that the μ-OH bridge accelerates the DNA cleavage as a nucleophile and the NH

group is essential for the hydrolytic DNA cleavage. The transition state in the DNA cleavage by **1a** is stabilized by DNA binding and protonation to the DNA binding complex. Mechanistic insights are proposed on the basis of these studies. The pH dependent activity control in the DNA cleavage of **1a** may provide some insights into the development of new cancer drugs to reduce the side effects.

This work was supported by MEXT-Supported Program of the Strategic Research Foundation at Private University, 2015–2019.

Supporting Information

X-ray structural data for the dicopper complexes, distances of *O*-atom of μ-OH bridge from the mean planes of **1a** and **2**, electronic absorption and ESI MS spectra in the complexation of ligands, DNA cleavage by **1a** in the presence of H_2O_2, NaN_3, or dmso, agarose gel electrophoresis profiles for all DNA cleavage studies, bond distances and angles for the dicopper complexes, data for the fractions of Form I, Form II, and Form III formed. This material is available on https://doi.org/10.1246/bcsj.20180353.

References

1 a) S. D. Kettenmann, F. R. Louka, E. Marine, R. C. Fischer, F. A. Mautner, N. Kulak, S. S. Massoud, *Eur. J. Inorg. Chem.* **2018**, 2322. b) T. J. P. McGivern, S. Afsharpour, C. J. Marmion, *Inorg. Chim. Acta* **2018**, *472*, 12. c) C. Santini, M. Pellei, V. Gandin, M. Porchia, F. Tisato, C. Cristina Marzano, *Chem. Rev.* **2014**, *114*, 815. d) S. Dasari, P. B. Tchounwou, *Eur. J. Pharmacol.* **2014**, *740*, 364. e) J. Qian, W. Gu, H. Liu, F. Gao, L. Feng, S. Yan, D. Liao, P. Cheng, *Dalton Trans.* **2007**, 1060. f) K. D. Copeland, M. P. Fitzsimons, R. P. Houser, J. K. Barton, *Biochemistry* **2002**, *41*, 343.

2 a) T. C. Johnstone, K. Suntharalingam, S. J. Lippard, *Chem. Rev.* **2016**, *116*, 3436. b) B. Rosenberg, *Cancer* **1985**, *55*, 2303.

3 Y. Kidani, K. Inagaki, M. Iigo, A. Hoshi, K. Kuretani, *J. Med. Chem.* **1978**, *21*, 1315.

4 M. J. McKeage, *Expert Opin. Investig. Drugs* **2001**, *10*, 119.

5 M. Shimada, H. Itamochi, J. Kigawa, *Cancer Manag. Res.* **2013**, *5*, 67.

6 a) D. Zhou, L. Shao, D. R. Spitz, *Adv. Cancer Res.* **2014**, *122*, 1. b) A. Weidemann, R. S. Johnson, *Cell Death Differ.* **2008**, *15*, 621. c) Y. Kato, S. Ozawa, C. Miyamoto, Y. Maehata, A. Suzuki, T. Maeda, Y. Baba, *Cancer Cell Int.* **2013**, *13*, 89.

7 a) R. J. Gillies, N. Raghunand, G. S. Karczmar, Z. M. Bhujwalla, *J. Magn. Reson. Imaging* **2002**, *16*, 430. b) A. Kondo, S. Yamamoto, R. Nakaki, T. Shimamura, T. Hamakubo, J. Sakai, T. Kodama, T. Yoshida, H. Aburatani, T. Osawa, *Cell Reports* **2017**, *18*, 2228. c) H. Lin, P. Herman, J. R. Lakowicz, *Cytometry* **2003**, *52A*, 77.

8 a) S. S. Massoud, C. C. Ledet, T. Junk, S. Bosch, P. Comba, R. Herchel, J. Hošek, Z. Trávníček, R. C. Fischer, F. A. Mautner, *Dalton Trans.* **2016**, *45*, 12933. b) L. J. K. Boerner, J. M. Zaleski, *Curr. Opin. Chem. Biol.* **2005**, *9*, 135.

9 D. Montagner, V. Gandin, C. Marzano, A. Erxleben, *J. Inorg. Biochem.* **2015**, *145*, 101.

10 a) C. A. Barta, S. R. Bayly, P. W. Read, B. O. Patrick, R. C. Thompson, C. Orvlg, *Inorg. Chem.* **2008**, *47*, 2280. b) A. C. Benniston, P. Gunning, R. D. Peacock, *J. Org. Chem.* **2005**, *70*, 115. c) S. Goswami, A. K. Das, A. K. Maity, A. Manna, K. Aich, S. Maity, P. Saha, T. K. Mandal, *Dalton Trans.* **2014**, *43*, 231. d) P. Chirakul, P. D. Hampton, Z. Bencze, *J. Org. Chem.* **2000**, *65*, 8297. e) D. A. Valyaev, S. Clair, L. Patrone, M. Abel, L. Porte, O. Chuzel, J.-L. Parrain, *Chem. Sci.* **2013**, *4*, 2815. f) J. M. Wilson, F. Giordani, L. J. Farrugia, M. P. Barrett, D. J. Robins, A. Suthrland, *Org. Biomol. Chem.* **2007**, *5*, 3651. g) E. Kimura, S. Aoki, T. Koike, M. Shiro, *J. Am. Chem. Soc.* **1997**, *119*, 3068.

11 A. W. Addison, T. N. Rao, J. Reedijk, J. v. Rijn, G. C. Verschoor, *J. Chem. Soc., Dalton Trans.* **1984**, 1349.

12 a) N. A. Rey, A. Neves, A. J. Bortoluzzi, C. T. Pich, H. Terenzi, *Inorg. Chem.* **2007**, *46*, 348. b) T. M. Rajendiran, R. Mahalakshmy, R. Kannappan, J. Rajeswari, R. Venkatesan, P. Rao, *Trans. Met. Chem.* **2003**, *28*, 280. c) P. Amudha, M. Kandaswamy, L. Govindasamy, D. Velmurugan, *Inorg. Chem.* **1998**, *37*, 4486.

13 a) C. R. Choudhury, S. K. Dey, R. Karmakar, C.-D. Wu, C.-Z. Lu, M. S. E. Fallah, S. Mitra, *New J. Chem.* **2003**, *27*, 1360. b) S. J. Smith, C. J. Noble, R. C. Palmer, G. R. Hanson, G. Schenk, L. R. Gahan, M. J. Riley, *J. Biol. Inorg. Chem.* **2008**, *13*, 499.

14 a) S. Torelli, C. Belle, I. Gautier-Luneau, J. L. Pierre, E. Sain-Aman, J. M. Latour, L. L. Pape, L. D. Luneau, *Inorg. Chem.* **2000**, *39*, 3526. b) J. Nagaj, K. Stokowa-Sołtys, E. Kurowska, T. Frączyk, M. Jeżowska-Bojczuk, W. Bal, *Inorg. Chem.* **2013**, *52*, 13927.

15 a) T. P. Szatrowski, C. F. Nathan, *Cancer Res.* **1991**, *51*, 794. b) V. Nogueira, N. Hay, *Clin. Cancer Res.* **2013**, *19*, 4309. c) G.-Y. Liou, P. Storz, *Free Radic. Res.* **2010**, *44*, 479.

16 a) E. Tuite, P. Lincoln, B. Nordén, *J. Am. Chem. Soc.* **1997**, *119*, 239. b) M. Eriksson, M. Leijon, C. Hiort, B. Nordén, A. Gräslund, *J. Am. Chem. Soc.* **1992**, *114*, 4933.

17 a) G. Manzini, M. L. Barcellona, M. Avitabile, F. Quadrifoglio, *Nucleic Acids Res.* **1983**, *11*, 8861. b) E. Tuite, U. Sehlstedt, P. Hagmar, B. Nordén, M. Takahashi, *Eur. J. Biochem.* **1997**, *243*, 482. c) P. Wittung, P. Nielsen, B. Nordén, *J. Am. Chem. Soc.* **1996**, *118*, 7049.

18 S. K. Kim, B. Nordén, *FEBS Lett.* **1993**, *315*, 61.

19 A. K. Williams, S. C. Dasilva, A. Bhatta, B. Rawal, M. Liu, E. A. Korobkova, *Anal. Biochem.* **2012**, *422*, 66.

20 W. D. Wilson, F. A. Tanious, H. J. Barton, L. Strekowski, D. W. Boykin, *J. Am. Chem. Soc.* **1989**, *111*, 5008.

21 a) B. C. Antanaitis, P. Aisen, *Adv. Inorg. Biochem.* **1983**, *5*, 111. b) D. C. Schlosnagle, F. W. Bazer, J. C. Tsibris, R. M. Roberts, *J. Biol. Chem.* **1974**, *249*, 7574.

22 G. Schenk, N. Mitić, G. R. Hanson, P. Comba, *Coord. Chem. Rev.* **2013**, *257*, 473.

23 G. Feng, D. Natale, R. Prabaharan, J. C. Mareque-Rivas, N. H. Williams, *Angew. Chem., Int. Ed.* **2006**, *45*, 7056.

24 P. Thaplyal, P. C. Bevilacqua, *Methods Enzymol.* **2014**, *549*, 189.

